Launch Vehicle Gust Penetration Loads

L. E. ERICSSON,* J. P. READING,† AND R. A. GUENTHER‡
Lockheed Missiles and Space Company, Sunnyvale, Calif.

The gust penetration loads on Saturn launch vehicles in sinusoidal gusts have been investigated. An analytic theory is presented that includes the effects of separated flow and associated convective time lag, and which accepts static experimental data as an input, thereby providing realistic gust load predictions. It is shown that the commonly used quasi-steady treatment that neglects the separated flow time lag can give very unconservative estimates of the gust induced loads even when experimental static load distributions are used. It will, however, give realistic gust load predictions for many launch vehicle geometries of practical interest.

Nomenclature

a = speed of sound, m/sec
c = reference length (maximum body diameter) m
f = gust function of inertial space coordinate X
L_b and L_g = body length and gust wavelength, m
M = Mach number, $M = U/a$
M_A = axial force generated pitching moment, kg-m coefficient $C_{m_A} = M_A/(\rho U^2/2)Sc$
M, N = maximum number of summation terms, Eqs. (14) and (16)
N = normal force, kg coefficient $C_N = N/(\rho U^2/2)S$
P = generalized force, kg-m/m, defined in Eq. (15)
$q(t)$ = amplitude, m of normalized bending deflection, $\delta = \varphi(x)q(t)$
S = reference area, m^2, $S = \pi c^2/4$
t = time, sec
t^* = time to reach maximum gust load, sec
U = vehicle velocity, m/sec
$\bar{U}$ = average wake velocity or boundary-layer convection velocity, m/sec
W_g = gust velocity normal to vehicle path, m/sec
X = inertial space coordinate, m (Fig. 4)
x = body fixed coordinate, m (Fig. 4)
Y = inertial space coordinate, m (Fig. 4)
y = body fixed lateral deflection, m
α = angle of attack, radians or degrees
δ = body deflection, m, $\delta = \varphi(x)q(t)$
Δ = amplitude or increment
θ = body pitch, radians or degrees
κ = time lag parameter defined in Eq. (14)
ρ = air density, kg-sec$^2/m^4$
$\varphi(x)$ = distribution of normalized bending mode deflection, $\delta = \varphi(x)q(t)$

Subscripts

a = attached flow
A = axial force
b = body
g = gust
i = numbering subscript for body station
L = local
max = maximum
N = nose
s = separated flow
o = apex of launch vehicle

Superscripts

i = induced, e.g., = separation induced normal force

Differential Symbols

$\varphi'(x) = \partial\varphi/\partial x$
$\dot{Y}(t) = \partial Y/\partial t$
$C_{N\alpha} = \partial C_N/\partial\alpha$
$C_{m\dot{\theta}} = \partial C_m/\partial(\dot{\theta}c/U)$

Introduction

As the size of the launch vehicles used in the manned space program has grown, long wavelength gusts have started to become of more and more concern. For the Saturn-I and Saturn-V boosters, so called sinusoidal gusts[1] can cause large gust penetration loads. Previous investigators[2-4] have assumed attached flow when defining the aerodynamic characteristics. This assumption is highly unrealistic. Flow separation occurs over much of the Saturn launch vehicles (Fig. 1). The multiple regions of separated flow have a dominant influence on the aerodynamic loads[5] (Fig. 2). Because of the separated flow time lag, the effect on the vehicle dynamics is even more dominant, as is illustrated by the damping of an early Saturn booster[5] (Fig. 3).

These results indicate that one cannot use attached flow estimates and expect to get a realistic assessment of the elastic vehicle dynamics. Likewise, when considering the gust response of the elastic vehicle, one should not expect realistic

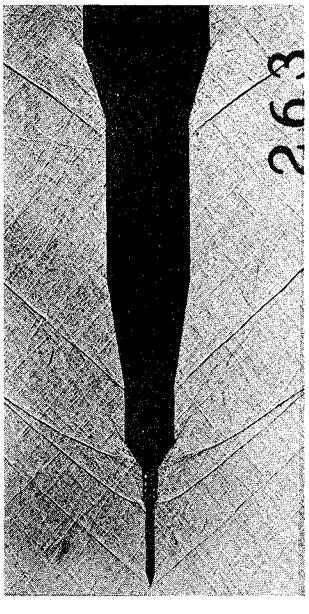

Fig. 1 Shadowgraph of flow over Saturn-V launch vehicle a $M = 1.46$.

Presented as Paper 71-178 at the AIAA 9th Aerospace Sciences Meeting, New York, January 25-27, 1971; submitted February 16, 1971; revision received September 7, 1971. The results were obtained in a study made for NASA Marshall Space Flight Center, Contract NAS 8-21459, under the direction of W. W. Clever.

Index Categories: Rocket Vehicle Gust Loading and Wind Shear; Nonsteady Aerodynamics; and Aeroelasticity and Hydroelasticity.

* Senior Staff Engineer. Associate Fellow AIAA.
† Research Specialist. Member AIAA.
‡ Senior Aerodynamics Engineer.

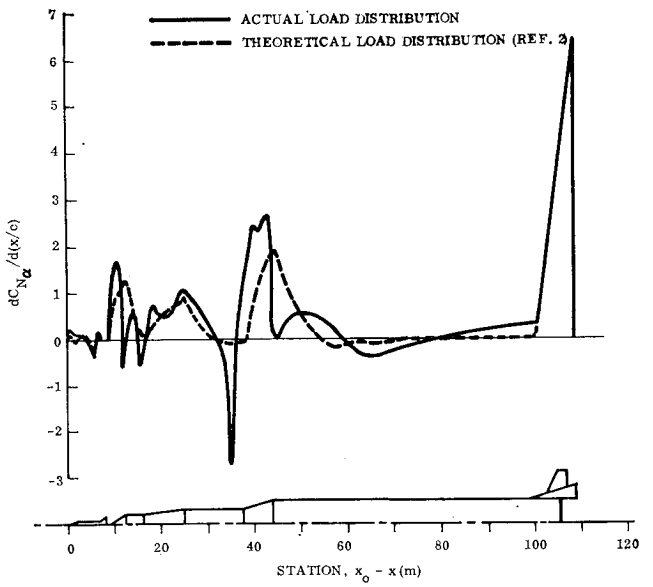

Fig. 2 Static load distribution on the Saturn-V launch vehicle at $M = 1.3$.

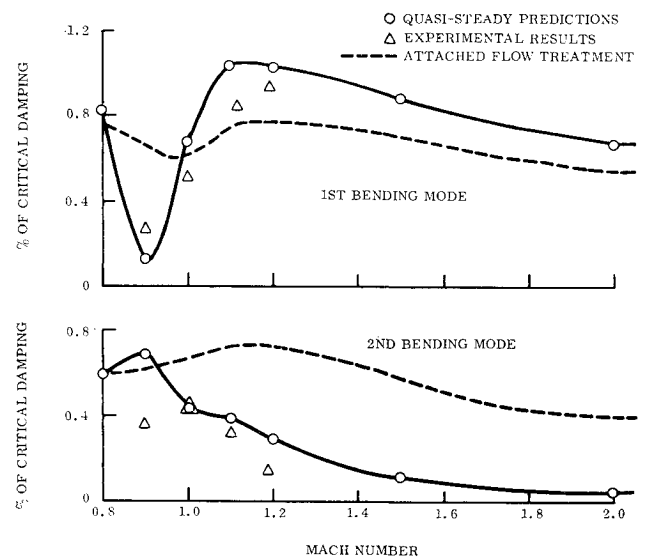

Fig. 3 Aerodynamic damping at $\alpha = 0$ of a Saturn-I launch vehicle with disk-on escape rocket.[8]

results unless the effects of flow separation are properly accounted for.

Analysis

The usual linearization approach is used, i.e., the environment is assumed to change slowly such that the time varying coefficients in the equations of motion can be represented by constant coefficients for finite time intervals in the trajectory. When the full coupled equations of motion are considered this procedure may not always be justified.

The present analysis is intended to assess the effects of sinusoidal gust on the structural loads of the elastic vehicle. As the total gust load can be determined by superposition,[6] only the linear analysis of one degree of freedom bending response to sinusoidal gusts will be discussed. The aerodynamic loads in regions of attached flow are determined by combining first-order momentum theory[7] with quasi-steady instantaneous load estimates[8,9] representing the cruciform fins by an equivalent cross-sectional area distribution.[2,8]

The local loads in separated flow regions are represented in a similar manner by an effective cross-sectional area.[10] The separation-induced loads are extracted from static experimental data and converted into dynamic loads using quasi-steady techniques that account for the effects of convective time lag[5,8,10,11] and accelerated flow.[12-14] The transverse gust velocity W_g and the vehicle velocity U are assumed to change negligibly during a time interval large enough to define the gust penetration load, e.g., the time interval required for the vehicle to travel one body length. Thus W_g is a function of the inertial space coordinate X only.

$$W_g = f(X - X_{go}) \tag{1}$$

With t_o = time of gust entry,

$$W_g = f(x, t - t_o) \tag{2}$$

For the time interval with constant vehicle velocity, the gust penetration depth is simply

$$X_o - X_{go} = (t - t_o)U \tag{3}$$

Or, with t set equal to zero at time of gust entry,

$$X_0 - X_{go} = Ut \tag{4}$$

Attached Flow Regions

In regions of attached flow, first-order momentum theory is used. It is assumed that the body is slender enough that the axial velocity over the vehicle surface deviates negligibly from the freestream velocity. The lift per unit length of the vehicle is then the reaction to the substantial rate of change of momentum of the virtual mass per unit length.[7] With the coordinate system of Fig. 4, the lift can be expressed as follows

$$dL/dX = -(d/dt)(dI/dX) = (U\,\partial/\partial X - \partial/\partial t)(dI/dX) \tag{5}$$

The momentum per unit length is

$$\begin{aligned} dI/dX &= -\rho A W = \rho A(dY/dt - W_g) \\ &= \rho A(\partial Y/\partial t - U\,\partial Y/\partial X - W_g) \end{aligned} \tag{6}$$

Thus,

$$dL/dX = (U\,\partial/\partial X - \partial/\partial t)[\rho A(-U\,\partial Y/\partial X + \partial Y/\partial t - W_g)] \tag{7}$$

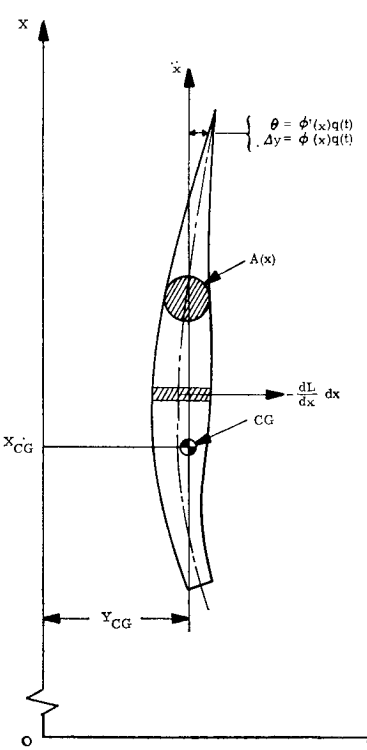

Fig. 4 Elastic body coordinate system.

With the gust stationary in space, $dWg/dt = O$, and Eq. (7) can be written

$$\frac{dL}{dX} = \left(U\frac{\partial}{\partial X} - \frac{\partial}{\partial t}\right)\left[\rho A\left(-U\frac{\partial Y}{\partial Y} + \frac{\partial Y}{\partial t}\right)\right] - \left[\left(U\frac{\partial}{\partial X} - \frac{\partial}{\partial t}\right)(\rho A)\right]W_g \quad (8)$$

With $L = (\rho U^2/2)SC_N (C_N = C_L$ for the small cross flow angles of interest), Eq. (8) can be expressed in the following form for time interval during which U and ρ remain constant.

$$\frac{dC_N}{dX} = \left(\frac{\partial}{\partial X} - \frac{1}{U}\frac{\partial}{\partial t}\right)\left[\frac{2A}{S}\left(-\frac{\partial Y}{\partial X} + \frac{1}{U}\frac{\partial Y}{\partial t}\right)\right] - \left[\left(\frac{\partial}{\partial X} - \frac{1}{U}\frac{\partial}{\partial t}\right)\frac{2A}{S}\right]\frac{Wg}{U} \quad (9)$$

Separated Flow Regions

A typical separated flow region on the Apollo-Saturn launch vehicles is sketched in Fig. 5. The flow is separating at x_N and reattaches at station x_a. The aerodynamic forces in the separated flow region forward of x_a are represented by lumped normal force and axial force (couple) moment vectors. In particular, the normal force N_s and axial force moment M_{A_s} generated on the conical frustum in the separated flowfield are dependent not only upon the local angle of attack α_s, but also upon the angle of attack α_N at the separated flow generator, and upon the relative displacement, $y = Y_N - Y_s$, between nose and frustum. For small angles of attack one can write N_s in the following linearized form (a similar expression is obtained for M_{A_s})

$$N_s = \frac{\rho U^2}{2} S\left\{\frac{\partial C_{N_s}}{\partial \alpha_s}\alpha_s + \frac{\partial C_{N_s}}{\partial \alpha_N}\alpha_N + \frac{\partial C_{N_s}}{\partial y}y\right\} \quad (10)$$

In the nonstationary case, α_N and Y_N (in $y = Y_N - Y_s$) are the values at a time increment Δt earlier than the instantaneous value for α_s, i.e.,

$$N_s(t) = \frac{\rho U^2}{2} S\left\{\frac{\partial C_{N_s}}{\partial \alpha_s}\alpha_s(t) + \frac{\partial C_{N_s}}{\partial \alpha_N}\alpha_N(t-\Delta t) + \frac{\partial C_{N_s}}{\partial y}[Y_N(t-\Delta t) - Y_s(t)]\right\} \quad (11)$$

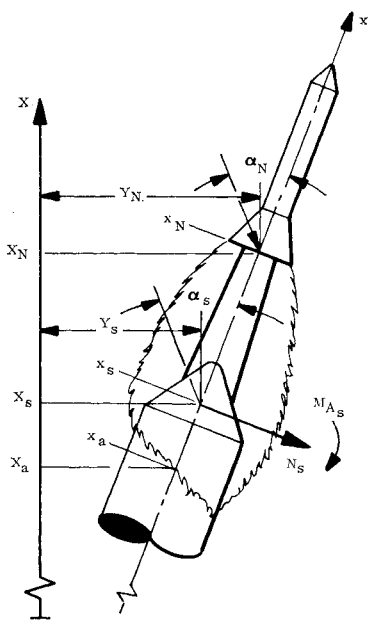

Fig. 5 Definition of separated flow parameters.

where $\Delta t = (x_N - x_s)/\bar{U}$. Δt is the time required for the force N_s to respond to changes in α_N and Y_N.

For determination of the gust penetration loads on the ascending rigid vehicle in Fig. 5, the variables α and y are as follows

$$\alpha = W_g/U; \quad y(t) = (x_N - x_s)\alpha(t - \Delta t) \quad (12)$$

Eq. (11) can then be written as follows

$$N_s(t) = \frac{\rho U^2}{2} S\left\{C_{N_{\alpha_L}}\frac{W_g(X_s,t)}{U} + \Delta^i C_{N_\alpha}\frac{W_g(X_N, t-\Delta t)}{U}\right\} \quad (13)$$

where

$$C_{N_{\alpha_L}} = \partial C_{N_s}/\partial \alpha_s; \quad \Delta^i C_{N_\alpha} = (x_N - x_s)\partial C_{N_s}/\partial y + \partial C_{N_s}/\partial \alpha_N$$

Thus, the gust penetration loads in the regions of separated flow on the Saturn-Apollo launch vehicle can be summed as follows

$$N_s + M_{A_s} = \sum_{i=1}^{N} N_{s_i}(t) + \sum_{i=1}^{M} M_{A_{s_i}}(t) \quad (14a)$$

$$N_{s_i}(t) = \frac{\rho U^2}{2} S\left\{C_{N_{\alpha_L}}\frac{W_g(Ut - [x_o - x_{s_i}])}{U} + \Delta^i C_{N_\alpha}(x_{s_i})\frac{W_g(Ut - [x_o - x_{is}]\kappa)}{U}\right\} \quad (14b)$$

$$M(A_{s_i})(t) = \frac{\rho U^2}{2} Sc\left\{C_{m_{\alpha_L}}(x_{s_i})\frac{W_g(Ut - [x_o - x_{s_i}])}{U} + \Delta^i C_{mA_\alpha}(x_{s_i})\frac{W_g(Ut - [x_o - x_{s_i}]\kappa)}{U}\right\} \quad (14c)$$

$$\kappa = 1 + (U/\bar{U} - 1)(x_{N_i} - x_{s_i})/(x_o - x_{s_i}) \quad (14d)$$

When the convection velocity in the separated flow region is not very different from the external (freestream) velocity, $\bar{U} \approx U$, $\kappa = 1$, the gust induced load depends only upon the total load, $C_{N_{\alpha_{\text{total}}}} = C_{N_{\alpha_L}} + \Delta^i C_{N_\alpha}$, and is independent of the composition of the load. That is, it does not matter whether the load is all induced, $C_{N_{\alpha_L}} = 0$, or all local, $\Delta^i C_{N_\alpha} = 0$. This in turn implies that the standard§ quasi-steady application of experimentally measured static load derivatives would give the correct gust induced load also in regions of separated flow.

The gust induced generalized force for one degree of freedom elastic vehicle bending is determined by the virtual work done by aerodynamic forces and moments.

$$P(t) = \int \frac{dN}{dx}\varphi(x)dx + \int \frac{dM_A}{dx}\varphi'(x)dx \quad (15)$$

In regions of separated flow this gust induced bending moment is determined as follows

$$P_s(t) = \sum_{i=1}^{N} N_{s_i}(t)\varphi(x_s) + \sum_{i=1}^{M} M_{A_{s_i}}(t)\varphi'(x_s) \quad (16)$$

$N_{s_i}(t)$ and $M_{A_{s_i}}(t)$ are defined by Eq. (14)

Discussion

The gust induced normal force on the Saturn-V is shown in Fig. 6 as a function of penetration depth into a sinusoidal gust. The maximum load is obtained after full penetration into the gust, and the transient load response at gust penetration does not produce the highest loads, as has also been observed by other investigators.[2,3] The variation of this maximum gust penetration load $|N|_{\max}$ with sinusoidal gust wavelength¶ is

§ In which separated flow time lag effects are neglected.

¶ L_b/L_g is the number of sinusoidal gust waves per body length.

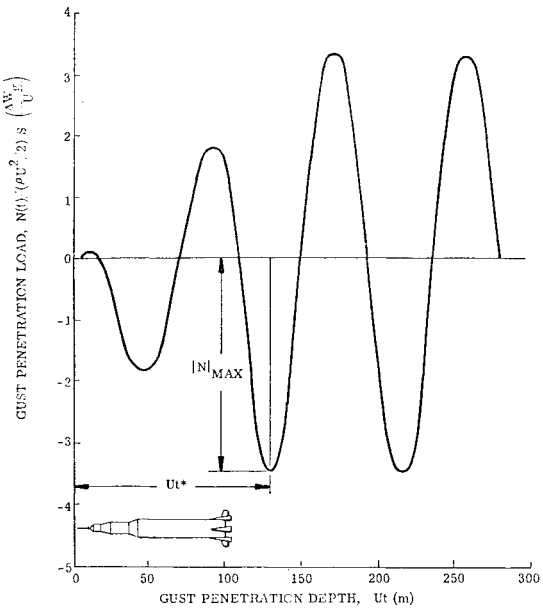

Fig. 6 Saturn-V gust induced normal force as a function of penetration depth into sinusoidal gust ($L_b/L_g = 1.05$) at maximum dynamic pressure ($M = 1.6$).

shown in Fig. 7. The actual position of the launch vehicle in the sinusoidal gust for peak and bottom values of $|N|_{max}$ are shown in the insets.

The effect of neglecting to account for the fact that the convection velocity is less than freestream velocity in regions of separated flow ($\kappa = 1$ compared to $\kappa \neq 1$) is negligible for the Saturn-V gust penetration load (Figs. 7 and 8). The Saturn-I launch vehicle exhibits similar characteristics when the escape rocket is the same (Fig. 9), but shows distinctly different characteristics when the escape rocket has a flow separation disk (Fig. 10). Not only is the κ-effect much larger, in addition, the largest load $|N|_{max}$ is no longer obtained for the (infinite penetration into a) step gust ($L_b/L_g = 0$), but for a gust with a wavelength of approximately 1.2 body length.[5]

The results for $\kappa = 1$ in Fig. 10 represent the results obtained if one uses static experimental load distributions in this standard type quasi-steady analysis.[4] As is seen, this will underestimate the actual maximum gust load at $L_b/L_g \approx 1.2$ by 40%. There are several reasons for the large gust loads and large κ-effects obtained with a disk-on escape rocket. The disk increases the escape rocket wake, thereby increasing the separation induced loads on the command module and

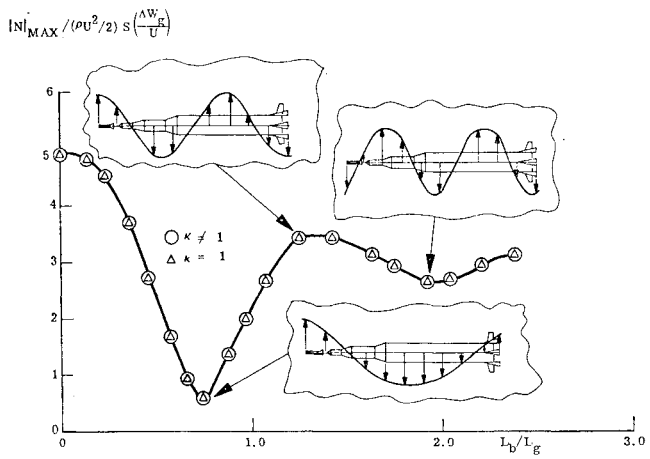

Fig. 7 Saturn-V maximum gust induced normal force as a function of gust wave length at $M = 1.6$.

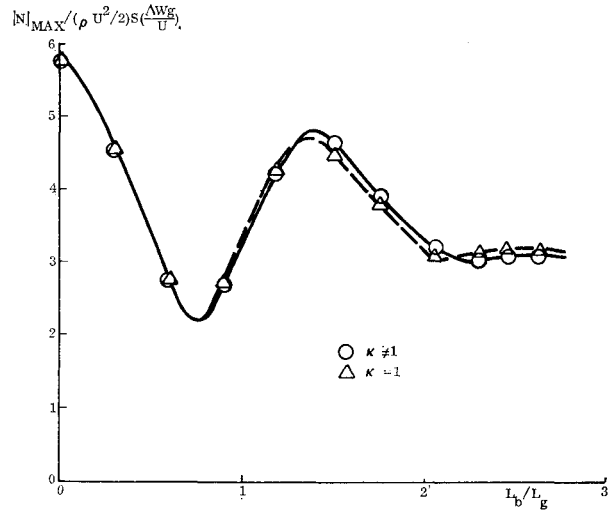

Fig. 8 Saturn-V maximum gust induced normal force as a function of gust wave length at $M = 0.9$.

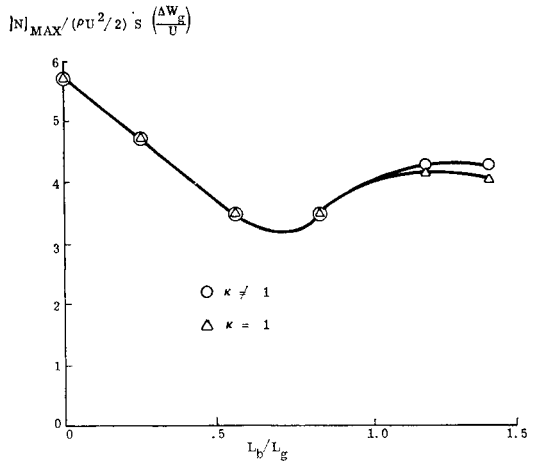

Fig. 9 Maximum gust induced normal force on the Saturn-I with disk-off escape rocket at $M = 0.9$.

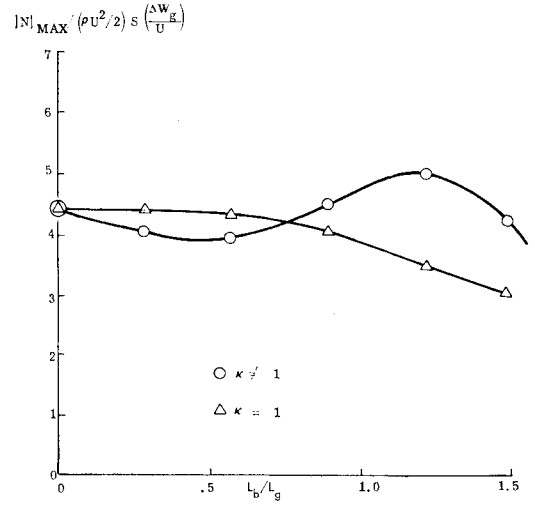

Fig. 10 Maximum gust induced normal force on the Saturn-I with disk-on escape rocket at $M = 0.9$.

forward service module[8] (Fig. 11). The larger velocity deficit in the wake causes a large increase of κ, especially at subsonic speeds (Fig. 12).

After all this display of large separated flow effects, it is surprising, to say the least, to find that the Saturn-V gust penetration load at maximum dynamic pressure is very well predicted by attached flow theory[2] (Fig. 13). It is obvious that the good agreement is fortuitous. The theoretical load distribution, although deviating very substantially from the measured distribution, gives the same total C_{N_z} (Fig. 2); and the maximum dynamic pressure occurs at a speed where the κ-effect is negligible (Fig. 7). As the wavelength decreases the difference in load distribution starts to show up ($L_b/L_g > 1.25$ in Fig. 13).

The gust induced bending loads for the first bending mode of the Saturn-V launch vehicle is shown in Fig. 14 as a function of the gust penetration depth. As for $|N|_{max}$ (Fig. 6), the maximum gust load is reached after full penetration into the sinusoidal gust. The variation of the maximum gust-induced bending $|P|_{max}$ with gust wavelength is shown in Figs. 15 and 16. As earlier for $|N|_{max}$, the κ-effect is negligible. The data

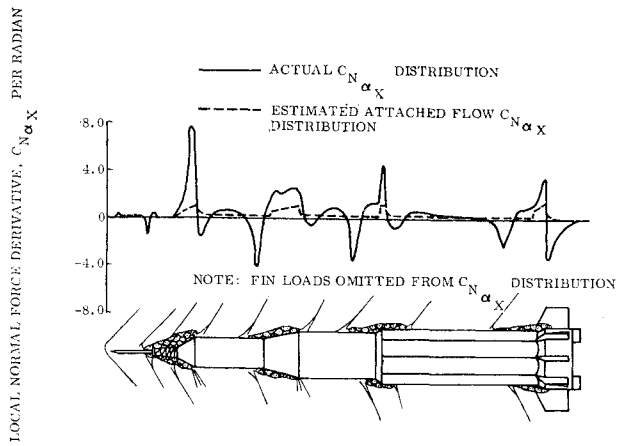

Fig. 11 Supersonic flowfield and normal force distribution for Saturn-I launch vehicle with disk-on.

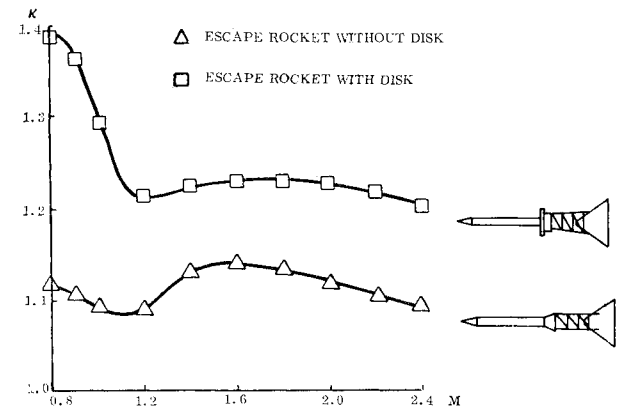

Fig. 12 Effect of flow separation disk-on κ for command module load.

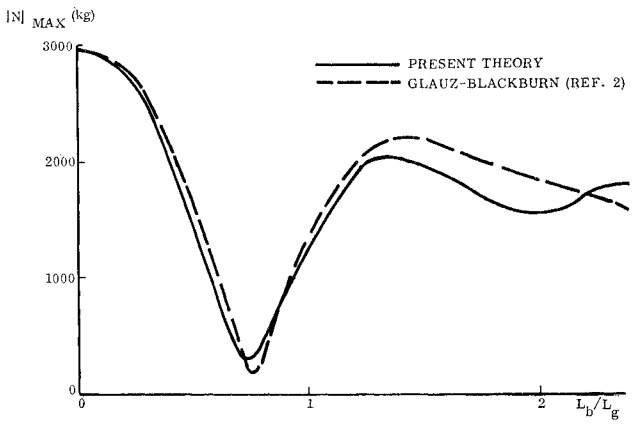

Fig. 13 Saturn-V gust induced normal force at maximum dynamic pressure ($M = 1.6$).

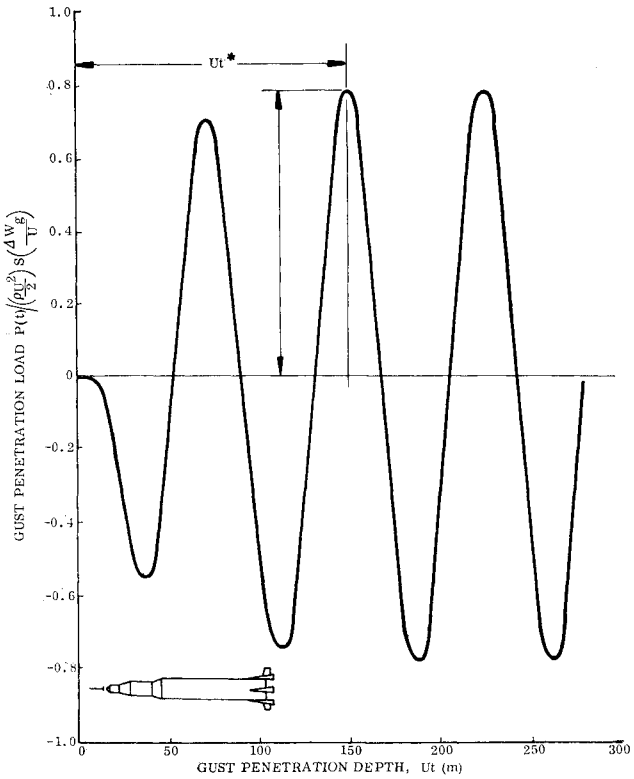

Fig. 14 Saturn-V gust induced bending loads (1st bending mode) at maximum dynamic pressure.

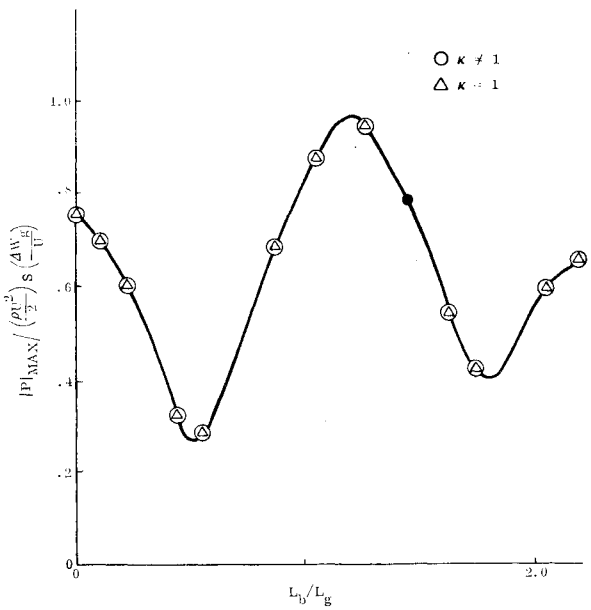

Fig. 15 Maximum elastic body gust induced bending on the Saturn-V at $M = 1.6$ (1st bending mode).

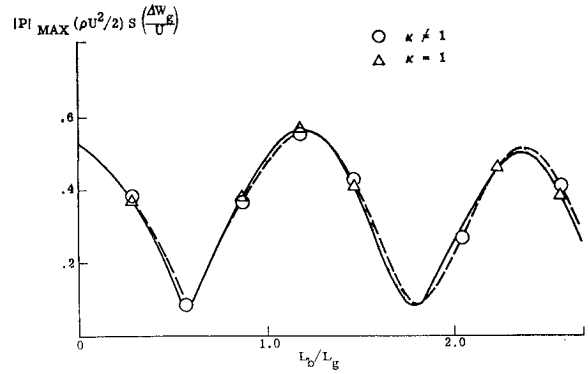

Fig. 16 Maximum elastic body gust induced bending on the Saturn-V at $M = 0.9$ (1st bending mode).

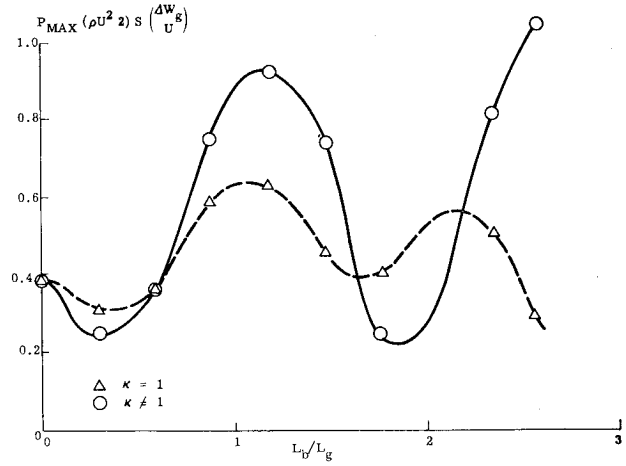

Fig. 18 Maximum elastic body gust induced bending on the Saturn-I launch-vehicle with disk-on escape rocket at $M = 0.9$ (1st bending mode).

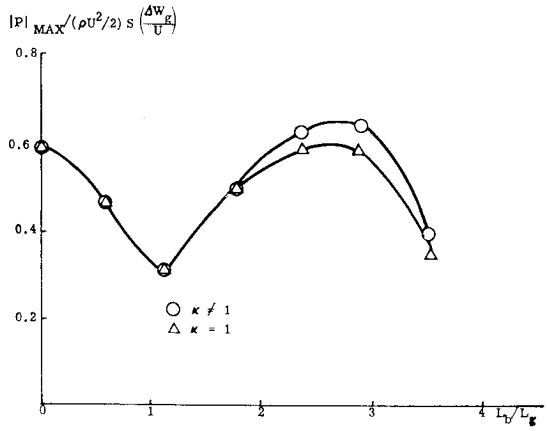

Fig. 17 Maximum elastic body gust induced bending on the Saturn-I with disk-off escape rocket at $M = 0.9$ (1st bending mode).

for Saturn-I is shown in Fig. 17. Figure 18 shows the gust induced bending for the Saturn-I with disk-on escape rocket. As earlier for $|N|_{max}$ (Figs. 9 and 10), the disk causes a large increase in the κ-effect, and reverses the wave length trend, i.e., gives the largest bending at short wavelengths (large L_b/L_g). The relatively larger effect of the disk on the gust induced bending than on the normal force (Figs. 17, and 18 compared to Figs. 9, and 10) is explained by the negative service module load (Fig. 19). At subsonic Mach numbers** the negative service module force forms together with the positive command module load a powerful force couple. It is obvious that this force couple will have a large effect on the gust induced bending loads, the effect being very sensitive to bending mode shape and gust wavelength.

It is seen that in many cases the standard quasi-steady theory[9] in combination with experimentally obtained static load distributions can provide a realistic estimate of the launch vehicle loads induced in sinusoidal gusts. However, this is not true when considering the elastic vehicle response to the gust loads.[15] The reason for this is that unconservative aerodynamic damping values are obtained if the separated flow time lag effects are neglected[5] (Fig. 3). The attached flow

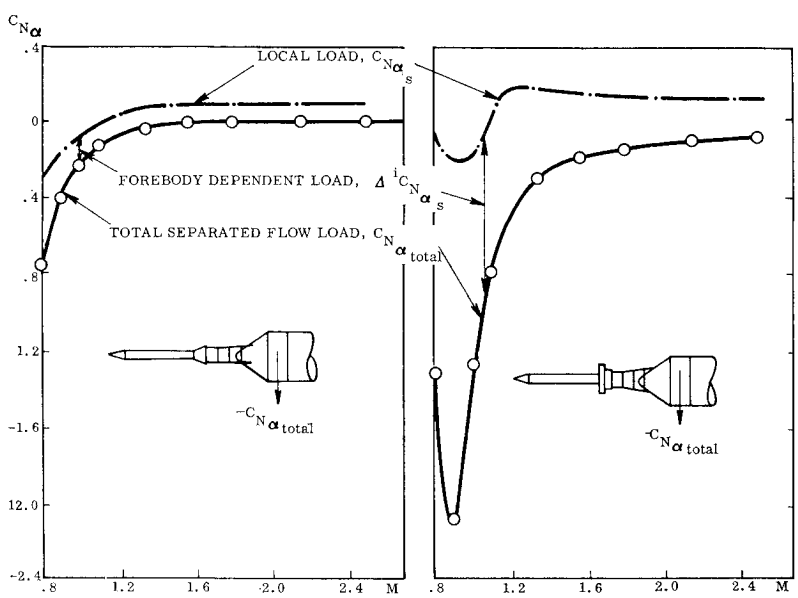

Fig. 19 Local and forebody-dependent negative command module shoulder loading.

**The positive command module force is much less Mach number sensitive.[8]

treatment data in Fig. 3 are obtained using static experimental data in combination with standard quasi-steady theory. When it is possible to describe the gust induced forcing function by the standard quasi-steady theory, the analysis is simplified greatly, something that can be appreciated when considering the space shuttle vehicles with their very much more complicated unsteady aerodynamic characteristics.[16]

Conclusions

A study of gust penetration loads on Saturn launch vehicles in sinusoidal gusts has given the following results: 1) The strongest effect of the separated flow is the distortion of the static load distribution; and 2) The effect of the separated-flow-induced time lag is less dominant. However, for vehicles with large separated flow regions its neglect can lead to highly unconservative estimates of the gust penetration loads, especially for the elastic vehicle. As a consequence, existing quasi-steady methods in combination with experimentally measured static load distributions will provide realistic estimates of gust penetration loads only when the separated flow time lag effects are small. This will, however, be true for many launch vehicle configurations of practical interest.

References

[1] Vaughn, W. W., "Sinusoidal Gust Criteria Guideline for Apollo Emergency Detection System Angular Rate Studies," Marshall Space Flight Center Memo R-AERO-Y-31-64, June 22, 1964, NASA.

[2] Glauz, W. D. and Blackburn, R. R., *Application of Theory to Basic Geometries and to the Saturn-V*, Vol. 1 of *Study of Indicial Aerodynamic Forces on Multistage Space Vehicle Systems*, Final Rept., June 1962–Sept. 1968, Contract NAS 8-21167, MRI Project 3089-P, Midwestern Research Inst., Kansas City, Mo.

[3] Blackburn, R. R. and St. John, A. D., "Effects and Importance of Penetration and Growth of Lift on Space Vehicle Response," AIAA Paper 67-608, Huntsville, Ala., 1967.

[4] Papadopoulos, J. G., "Wind Penetration Effects on Flight Simulation," AIAA Paper 67-609, Huntsville, Ala., 1967.

[5] Ericsson, L. E. and Reding, J. P., "Analysis of Flow Separation Effects on the Dynamics of a Large Space Booster," *Journal of Spacecraft and Rockets*, Vol. 2, No. 4, July–Aug. 1965, pp. 481–490.

[6] Lester, H. C. and Morgan, H. G., "Determination of Launch Vehicle Response to Detailed Wind Profiles," *Journal of Spacecraft and Rockets*, Vol. 2, No. 1, Jan.–Feb. 1965, pp. 62–67.

[7] Bisplinghoff, R. L., Ashley, H., and Halfman, R. L., *Aeroelasticity*, Addison–Wesley, Cambridge, Mass., 1955, pp. 418–419.

[8] Ericsson, L. E. and Reding, J. P., "Report on Saturn-I—Apollo Unsteady Aerodynamics," LMSC–A650215, Contract NAS 8–5338, Feb. 1964, Lockheed Missiles and Space Co., Sunnyvale, Calif.

[9] Wells, C. R. and Mitchell, H. P., "A Mathematical Model for Flexible Response of Uprated Saturn-I Inflight Winds," *Journal of Spacecraft and Rockets*, Vol. 5, No. 3., March 1968, pp. 313–320.

[10] Ericsson, L. E. and Reding, J. P., "Aeroelastic Characteristics of Saturn-IB and Saturn-V Launch Vehicles," TR M-37-67-5, Contract NAS 8-11238, Dec. 1967, Lockheed Missiles and Space Co., Sunnyvale, Calif.

[11] Ericsson, L. E. and Reding, J. P., "Dynamics of Separated Flow over Blunt Bodies," TR 2-80-65-1, Contract NAS 8-5338, Dec. 1965, Lockheed Missiles and Space Co., Sunnyvale, Calif.

[12] Ericsson, L. E., Reding, J. P., and Guenther, T. A., "Effects of Shock-Induced Separation," TR L-87-69-1, Contract NAS 8-20354, June 1969, Lockheed Missiles and Space Co., Sunnyvale, Calif.

[13] Ericsson, L. E., "Aeroelastic Instability Caused by Slender Payloads," *Journal of Spacecraft and Rockets*, Vol. 4, No. 1, Jan. 1967, pp. 65–73.

[14] Ericsson, L. E., "Loads Induced by Terminal-Shock Boundary-Layer Interaction on Cone-Cylinder Bodies," *Journal of Spacecraft and Rockets*, Vol. 7, No. 9, Sept. 1970, pp. 1106–1112.

[15] Ericsson, L. E., Reding, J. P., and Guenther, R. A., "Gust Penetration Loads and Elastic Vehicle Response for Saturn-V Launch Vehicles," TR N-3C-70-2, Contract NAS 8-21459, July 1970, Lockheed Missiles and Space Co., Sunnyvale, Calif.

[16] Reding, J. P. and Ericsson, L. E., "Unsteady Aerodynamics of Manned Space Vehicles: Past, Present, and Future," *Transactions of the First Western Space Congress*, Pt. II, Santa Maria, Calif. Oct. 27–29, 1970, pp. 882–893.